Title

Quantitative biophysical analysis defines key components modulating recruitment of the GTPase KRAS to the plasma membrane

Permalink

Journal

ISSN

Authors

Lakshman, Bindu
Messing, Simon
Schmid, Eva M
et al.

Publication Date

DOI

Peer reviewed

Quantitative biophysical analysis defines key components modulating recruitment of the GTPase KRAS to the plasma membrane

Bindu Lakshman[‡], **Simon Messing**[‡], **Eva M. Schmid**[§], **Jeffrey D. Clogston**[¶], **William K. Gillette**[‡], **Dominic Esposito**[‡], **Bailey Kessing**[‡], **Daniel A. Fletcher**[§‖**], **Dwight V. Nissley**[‡], **Frank McCormick**[‡‡‡], **Andrew G. Stephen**[‡], and **Frantz L. Jean-Francois**[‡1]

From the ‡*NCI RAS Initiative, Cancer Research Technology Program, Frederick National Laboratory for Cancer Research, Leidos Biomedical Research, Inc., Frederick, Maryland 21702,* §*Department of Bioengineering, University of California Berkeley, Berkeley, California 94720,* ¶*Nanotechnology Characterization Laboratory, Cancer Research Technology Program, Leidos Biomedical Research, Inc., Frederick National Laboratory for Cancer Research, Frederick, Maryland, 21702,* ‖*Division of Biological Systems and Engineering, Lawrence Berkeley National Laboratory, Berkeley, California 94720,* *******Chan Zuckerberg Biohub, San Francisco, California 94158,* ‡‡*Helen Diller Family Comprehensive Cancer Center, University of California, San Francisco, California 94158*

Edited by Karen G. Fleming

The gene encoding the GTPase KRAS is frequently mutated in pancreatic, lung, and colorectal cancers. The KRAS fraction in the plasma membrane (PM) correlates with activation of the mitogen-activated protein kinase (MAPK) pathway and subsequent cellular proliferation. Understanding KRAS's interaction with the PM is challenging given the complexity of the cellular environment. To gain insight into key components necessary for KRAS signal transduction at the PM, we used synthetic membranes such as liposomes and giant unilamellar vesicles. Using surface plasmon resonance (SPR) spectroscopy, we demonstrated that KRAS and Raf-1 proto-oncogene Ser/Thr kinase (RAF1) domains interact with these membranes primarily through electrostatic interactions with negatively charged lipids reinforced by additional interactions involving phosphatidyl ethanolamine and cholesterol. We found that the RAF1 region spanning RBD through CRD (RBDCRD) interacts with the membrane significantly more strongly than the isolated RBD or CRD domains and synergizes KRAS partitioning to the membrane. We also found that calmodulin and phosphodiesterase 6 delta (PDE6δ), but not galectin3 previously proposed to directly interact with KRAS, passively sequester KRAS and prevent it from partitioning into the PM. RAF1 RBDCRD interacted with membranes preferentially at nonraft lipid domains. Moreover, a C-terminal O-methylation was crucial for KRAS membrane localization. These results contribute to a better understanding of how the KRAS–membrane interaction is tuned by multiple factors whose identification could inform drug discovery

efforts to disrupt this critical interaction in diseases such as cancer.

The GTPase KRAS is frequently mutated in pancreatic (98%), lung (31%), and colorectal cancer (45%) [1]. RAS GTPases are implicated in cellular proliferation through activation of the MAPK[2] pathway. They are primarily anchored at the membrane through lipidated hypervariable regions (HVR) which are responsible for localization to specific microdomains [2, 3]. A RAS anchor consists of two components: a C-terminal S-farnesyl cysteine carboxymethyl ester, common to all isoforms, and a second determinant that comprises mono-palmitoylation of NRAS and KRAS4A, duo-palmitoylation of HRAS, and a polybasic domain of six lysines in KRAS4B, the predominantly expressed splice variant of KRAS, hereafter referred to as KRAS.

The PM is the boundary of the cell, separating the cell from its surroundings. It is a dynamic and heterogeneous cellular subsystem as it interacts with proteins that perform a myriad of different functions necessary for regulating cellular processes, interacting with external environment or neighboring cells, or responding to stimuli. Many cytoplasmic proteins are recruited to the PM and other cellular membranes during cell signaling and membrane trafficking. These proteins are collectively known as peripheral proteins (as opposed to integral membrane proteins) or amphitrophic proteins. Peripheral proteins

[2] The abbreviations used are: MAPK, mitogen-activated protein kinase; CRD, cysteine-rich domain; DPPC, 1,2-dipalmitoyl-sn-glycero-3-phosphocholine; DPPS, 1,2-dipalmitoyl-sn-glycero-3-phospho-L-serine sodium salt; DOPA, 1,2-dioleoyl-sn-glycero-3-phosphate sodium salt; DOPC, 1,2-dioleoyl-sn-glycero-3-phosphocholine; DOPE, 1,2-dioleoyl-sn-glycero-3-phosphoethanolamine; DOPS, 1,2-dioleoyl-sn-glycero-3-phospho-L-serine sodium salt; GUV, giant unilamellar vesicle; HVR, hypervariable region; Ld, liquid disordered; LUV, large unilamellar vesicle; MEK, mitogen-activated protein kinase; PA, phosphatidic acid; PE, phosphatidylethanolamine; PIP2, L-α-phosphatidyl-inositol-4,5-bisphosphate ammonium salt; PM, plasma membrane; POPC, 1-palmitoyl-2-oleoyl-sn-glycero-3-phosphocholine; POPS, 1-palmitoyl-2-oleoyl-sn-glycero-3-phospho-L-serine sodium salt; PS, phosphatidylserine; RBD, ras-binding domain; SPR, surface plasmon resonance.

SASBMB
Published in the U.S.A.

J. Biol. Chem. (2019) 294(6) 2193–2207 **2193**

use different strategies for reversible membrane interactions. Many peripheral proteins contain one or more modular domains specialized in lipid binding. These lipid-binding structural modules, also known as membrane-targeting domains, include PKC conserved 1 (C1); PKC conserved 2 (C2); pleckstrin homology (PH); Fab1, YOTB, Vac1, and EEA1 (FYVE); Phox (PX); epsin N-terminal homology (ENTH); AP180 N-terminal homology (ANTH); Bin amphiphysin Rvs (BAR); band 4.1, ezrin, radixin, moesin (FERM); and tubby domains (4).

In the case of the MAP kinase pathway, KRAS and RAF1 come together at the PM to give rise to an activated RAF1 through a set of mechanisms which are still not fully understood. Here a reductionist approach is used to exclusively identify individual behavior and interaction with a limited number of components. KRAS has been shown to interact preferentially with negatively charged lipid in a fluid phase (5, 6). KRAS/RAF localization to the membrane is the main step that drives activation of the MAPK signaling pathway. In this study, we perform a quantitative membrane interaction analysis of KRAS and RAF1 domains to decipher the key components modulating KRAS/RAF1 interplay at the membrane and understand their involvement in the MAPK pathway activation (7–9). Here we use a combination of qualitative confocal imaging data and quantitative parameters extracted from surface plasmon resonance SPR data (10, 11) such as membrane-associated protein fractions, kinetics of desorption, partition coefficients, and membrane stoichiometry to systematically interrogate KRAS and RAF1 interaction with artificial membranes. We assessed the impact of lipid compositions variation and quantified the impact of various binding partners and posttranslational modification on KRAS membrane interaction.

Results

Quantitative SPR analysis

Mathematical models were used to allow quantification of the SPR sensorgrams and subsequent biological conclusions. The previously described steady-state and dissociation models were used as a basis (11). They were further implemented with free energy and membrane-associated protein fraction calculations to allow representation of the fractional membrane-associated values with respect to the free energy of membrane partitioning. A new formalism is also described to extract the average amount of protein adsorbed at the surface of individual liposomes. All equations and rationale for the SPR data analysis are detailed below.

Free energy and fraction of membrane-associated proteins— The mathematical model described by Figueira *et al.* (11), specifically Equations 1 and 2, was applied to calculate the partition coefficient from the SPR sensorgrams shown in Equation 1:

$$\frac{RU_S}{RU_L} = \gamma_L K_P \frac{M_S}{M_L} [S]_w \tag{1}$$

where RU_S and RU_L, respectively, are the solute membrane association response unit and the total lipid deposition response; γ_L is the lipid molar volume; K_P is the partition coefficient and $[S]_w$ is the solute concentration in the aqueous phase;

and M_S and M_L are the molecular mass of the solute and lipids, respectively.

For some data sets, Equation 2, also from Figueira *et al.* (11), allowed the determination of the lipid-to-solute ratio.

$$\frac{RU_S}{RU_L} = \frac{\gamma_L K_P \frac{M_S}{M_L} [S]_w}{1 + \sigma \gamma_L K_P [S]_w} \tag{2}$$

where σ is the lipid:solute molar ratio at membrane saturation.

The Gibbs free energy of the protein transfer from the aqueous phase into the lipid phase is then calculated using Equation 3:

$$\Delta G^\circ = -RT \ln K_P \tag{3}$$

where R is the universal gas constant and T is the absolute temperature.

To calculate the fraction of membrane-associated protein per vesicle for each of the lipid:protein combinations, Equation 4 was applied:

$$f_b = \frac{K_P [L]}{55.6 + K_P [L]} \tag{4}$$

Here, [L] is half of the total lipid concentration (M) at the surface of the chip. In fact, the proteins used here cannot permeate the bilayer and can therefore only partition to the outer leaflet. 55.6 = the molar concentration of water.

Residence time—Protein half-life values on various liposomes were obtained following the dissociation formalism of Figueira *et al.* (11) seen in Equations 5 and 6:

$$S_L(t) = \alpha e^{-k_{off,\alpha}t} + \beta e^{-k_{off,\beta}t} + S_{L,r} \tag{5}$$

and

$$\langle k_{off} \rangle = \frac{\alpha k_{off,\alpha} + \beta k_{off,\beta}}{\alpha + \beta} \tag{6}$$

Here, $S_L(t)$ is the membrane-associated solute fraction at a given time, t; $S_{L,r}$ is the retained solute fraction at $t = \infty$; α and β are the fractional contribution of each population; and $\langle k_{off} \rangle$ is the weight-averaged rate of membrane release. For a given dissociation time $t = \tau$, $S_L(\tau)$ was obtained using the linearized formalism of Figueira *et al.* shown in Equation 7:

$$RU_{S,diss}(\tau, [S]_w) = \frac{S_L(\tau)}{1 - S_L(\tau)}(RU_{S,max}([S]_w) - RU_{S,diss}(\tau, [S]_w)) \tag{7}$$

where $RU_{S,diss}$ and $RU_{S,max}$ correspond to the sensorgram dissociation response values and the maximum association response values, respectively.

Stoichiometry—Conventional SPR formalism at the steady state was used to determine the average amount of protein adsorbed at the surface of individual liposomes as seen in Equation 8:

$$N = \frac{RU_S M_{Lipo}}{RU_L M_S} \tag{8}$$

Here, N is the number of solute molecules adsorbed at the membrane. M_{Lipo}, the molecular weight of a liposome, is calculated using Equation 9:

$$M_{lipo} = \frac{\left[4\pi\left(\frac{d}{2}\right)^2 + 4\pi\left(\frac{d}{2} - h\right)^2 \right]}{a} \times M_L \qquad (9)$$

where $4\pi(d/2)^2$ is the surface of one of the monolayers of the liposome, d is the diameter of the liposome, h is the thickness of the bilayer, and a is the lipid headgroup area of one lipid molecule. For the calculated stoichiometries, the above equation was simplified to a DOPC containing liposome only using Equation 10:

$$M_{lipo} = 17.69 \times \left[\left(\frac{d}{2}\right)^2 + \left(\frac{d}{2} - 5\right)^2 \right] \times M_L \qquad (10)$$

KRAS lipid preference

The importance of negatively charged lipids in KRAS membrane adsorption is well-documented (12). KRAS interactions with other lipid headgroups have been less extensively studied. To determine the relative importance of lipid headgroups in KRAS membrane interaction, the seven most abundant lipid headgroups were incorporated in liposomes. The same dioleoyl acyl chain was chosen for all phospholipids to allow direct comparison of specific headgroup effects. A dioleoyl aliphatic tail ensures that at experimental temperatures all liposomes are in a liquid disordered (Ld) fluid phase (13). Relative proportions of incorporated lipids were determined based on a Madin-Darby canine kidney cell plasma membrane lipidomic analysis (14). Available knowledge of flippase-driven asymmetry between the inner and outer leaflets (15) was used to adjust our lipid compositions L3 to L10 as reported in Table 1. Hereafter the various liposome compositions will be referred by their number in Table 1. Liposomes L1 to L10 were used to analyze headgroup-specific interactions. Among them, 9 of 10 lipid compositions were designed to have an estimated 30% negative net charge, allowing determination of specific headgroup preferences beyond the well-established electrostatic interaction between the polybasic HVR and acidic lipids (16). By duplicating one lipid composition (L6 and L8), we incorporated a technical replicate that was used as a control in all experiments. Some liposome mixtures were characterized using HPLC-CAD which confirmed incorporation of most lipids. Only PIP2, notoriously difficult to incorporate in liposomes, incorporated below the 0.3% CAD detection limit (Table 1 and Fig. S1).

KRAS exhibits good association and dissociation behavior for most lipid compositions as displayed on Fig. 1A for L6. Analysis of the fractions of membrane-associated protein shows a charge-based distribution (Fig. 1, B and C). All charged liposomes showing good partition at the membrane (~80 to over 90% membrane associated) whereas the neutral L1 composition is only 13% membrane associated. At 30% charge we calculated ~8 kJ/mol difference in partitioning energy between noncharged and charged membranes, similar to values that had been reported previously (17). This representation confirms that even small contributions to the partitioning energy can

shift the fraction of membrane-associated KRAS protein significantly. It is to be noted that liposomes containing the phosphatidic acid (PA) headgroup (L2) yielded a slightly lower partition in the membrane than liposomes containing PS (L3) suggesting a stronger contribution of PS over PA at similar net charge (Fig. 1, B and C). Various compositions of lipid headgroups gave rise to specific dissociation patterns. For all compositions a rapid dissociation in the order of seconds is observed. Membrane dissociation of farnesylated peptides in the order of seconds was observed previously with intervesicle exchange experiments (18, 19). With this more quantitative analysis we show that KRAS displays a single fast-dissociating population with a half-life of 7 s from neutral L1 lipids. For all negatively charged liposomes, however, two populations of fast and slow dissociation rates were observed (Fig. 1, D and E and Table S1).

Interestingly, Fig. 1D and Table S1 show a gradual increase in the weight-averaged dissociation half-life from lipid compositions L2–L3 containing only PS or PA (~16 s) to the ones containing PS, PE, and cholesterol L4–L9 (~27 s). Although the slow dissociating KRAS population is generated by addition of negatively charged lipids, its ratio (~0.6) appears doubled with respect to the negatively charged lipids molar ratio (~0.3). To further analyze the effect of the lipid headgroups, Equations 2 and 8 were used to calculate KRAS stoichiometry and lipid-to-solute ratios σ. Fig. 2A shows that the two PS-containing lipid compositions L3 and L5, which are cholesterol free, can accommodate more KRAS molecules (~3500 versus ~2300) and thus showed low σ values of 47 (Table S3). The same observation was made with the HVR (data not shown). Beyond the headgroup selectivity, acyl chains were also investigated. Maintaining a 30% net charge with a PS headgroup, various acyl chains were used to generate specific lipid phases. Results show a significant impact of acyl chain variations on KRAS membrane adsorption (Fig. 2C). Acyl chain yielding fluid phase such as L3 led to good KRAS membrane partitioning, with over 90% of the protein at the membrane. Whereas acyl chains forming liquid-ordered (L14) or gel phases (L13) led to no partitioning of KRAS in the membrane despite their overall net negative charges. These relative partitioning values for various lipid phases correlate well with the available data published. In a recent study by Hancock and co-workers (12), when 1,2-distearoyl-sn-glycerol-3-phospho-L-serine (DSPS) was added exogenously into cells depleted in PS lipids, which favors gel- or liquid-ordered phases formation, there was significant reduction in the localization of KRAS to the PM. Winter and co-workers had also shown poor KRAS membrane translocation in GUVs containing PS liquid-ordered regions (6, 20–22). These results were obtained using a semisynthetic version of KRAS, however. We reproduced these results using fully processed eGFP-KRAS and showed how electrostatic interactions affect KRAS partitioning (Fig. 2D, upper panel). More subtle differences such as the importance of asymmetric lipid tails were also suggested to have an impact on KRAS nanoclustering and membrane localization outcomes (12). Our results yielded equivalent KRAS membrane partitioning for the symmetric lipid DOPS (L3) versus asymmetric POPS (L18) lipid and a slight increase in KRAS stoichiometry per liposome at saturation is noticed for the asymmetric POPS (Fig. S3). To further analyze the effect of the

ᕮASBMB

J. Biol. Chem. (2019) 294(6) 2193–2207 **2195**

Table 1
Lipid compositions
Moles percentages of each lipid per liposome composition. Measured values are in parentheses. Liposome phases are displayed. *Ld*: lamellar liquid disordered, *Lo*: lamellar liquid ordered, *Pβ′*: gel rippled. Liposome net charges at pH 7.4 were determined based on estimated mole percentages based on lipid headgroup pKa. Calculated ζ potentials are displayed. S.D. based on averages of three measurements are in parentheses. Hydrodynamic size reported refers to the diameter as measured by dynamic light scattering (DLS), *error bars* ~ ± 3 nm. Lipid compositions L11 and L12 were prepared only as giant vesicles; therefore, their size exceeded microns, and DLS measurements are not applicable (NA). Cells were left empty when the corresponding lipid (column) was not added to a specific liposome composition (row).

#	DOPC	DOPS	Chol	DOPE	DOPA	PSM	PIP2	ZP (mV)	Phase	Net charge	Size (nm)
L1	100							-3.4 ± 0.2	Ld	0	133
L2	77 (74)			23 (26)				-9.9 ± 0.8	Ld	-30	126
L3	70 (71)	29						-10.2 ± 0.3	Ld	-30	150
L4	45 (48)	31	21					-9.9 ± 1.5	Ld	-30	148
L5	40	30	0	30				-9.9 ± 1.6	Ld	-30	145
L6	15 (34)	30 (30)	25 (12)	30 (24)				-11.5 ± 0.8	Ld	-30	133
L7	30	30	25	15				-11.0 ± 1.9	Ld	-30	131
L8	15 (34)	30 (30)	25 (12)	30 (24)				-15.1 ± 3.6	Ld	-30	139
L9	11	21	25	30		10	3	-12.0 ± 0.7	Ld	-30	148
L10	11.4 (26)	19 (28.6)	25 (12.6)	30 (27.2)	1.54 (1)	10 (4.2)	3 (<0.3)	-10.9 ± 1.7	Ld	-30	148

#	DOPC	DOPS	DPPC	DPPS	Chol	Ceramide	POPC	POPS	Phase	Net charge	Size (nm)
L11	10	15	35	15	25				Ld + Lo	-30	NA
L12	25		50		25				Ld + Lo	0	NA
L13			70	30					Pβ'	-30	159
L14			45	30	25				Lo	-30	127
L15	90 (94)					10 (6)			Ld	0	168
L16	80 (90)					20 (10)			Ld	0	176
L17							100		Ld	0	154
L18							70	30	Ld	-30	138

side chain, the experiments were performed at 37 °C. Higher temperature increases disorder of the lipid aliphatic chains leading to less partitioning in the membrane (Fig. S3).

RAF1 domains (RBD, CRD, and RBDCRD) lipid preference

RAF1 kinase is known to interact with the plasma membrane via the cysteine-rich domain (23, 24). We carried out a series of membrane partitioning analyses using three segments of RAF1 kinase to interrogate their ability to partition in synthetic membranes and determine their relative contribution to partitioning. RAF1 kinase fragments, RBD (RAF1 52–131), CRD (RAF1 136–188), and RBDCRD (RAF1 52–188) were expressed and purified. Because PS (23, 24) and PA (23, 25) were previously reported to contribute to RAF1 membrane partitioning, the same 10 lipid compositions (L1–L10) were used to test their

relative partitioning into inner leaflet mimicking model membranes. Using Equation 8, RBDCRD stoichiometry per liposome was calculated and displayed on Fig. 2B. Membrane fraction calculation of the RAF1 fragments unexpectedly revealed a striking difference for RBDCRD compared with individual domains of RBD and CRD. Seventy-five percent of RBDCRD partitions into the negatively charged L6 membrane, whereas only 4% of RBD and 19% of CRD bind to L6 (Fig. 2E). As RBDCRD displayed the most significant partitioning, a thorough analysis of its lipid preferences was performed (Fig. 3). Akin to KRAS, RBDCRD exhibits good association and dissociation behavior as displayed on Fig. 3A. As expected, the interaction is electrostatically driven, as only the noncharged DOPC liposomes showed no partitioning. Liposomes containing high amounts of DOPE and cholesterol showed highest partitioning
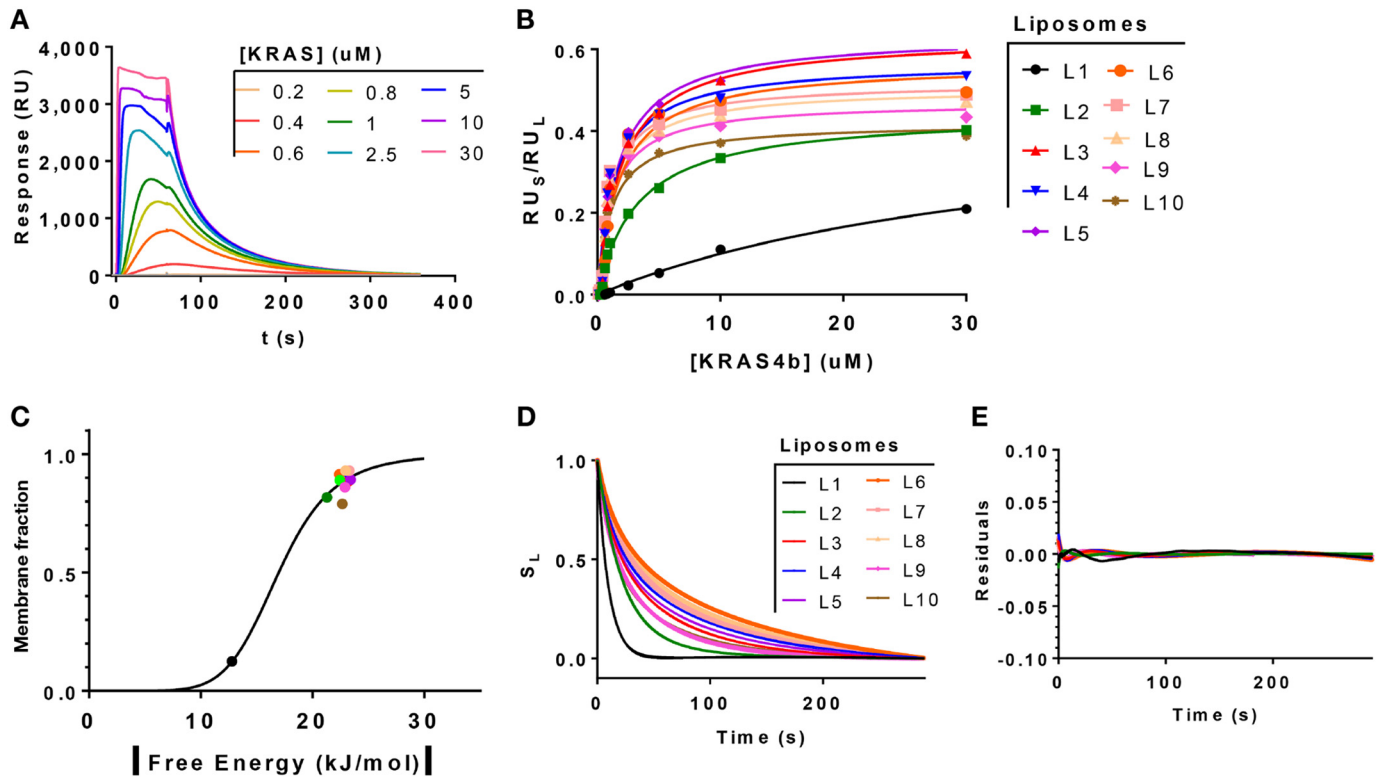
Figure 1. KRAS interaction with liposomes. *A*, SPR sensorgrams for KRAS partitioning into liposome L6. A baseline correction was applied to remove the retained fraction. *B*, binding isotherms for liposomes L1 to L10. RU_S values were collected from individual sensorgrams at 60 s of the association phase for each concentration. The RU_S values are displayed relative to RU_L values at each concentration for liposomes L1 to L10. *C*, fraction of membrane-associated KRAS protein as a function of the absolute unitary Gibbs free energy of transfer from the aqueous phase into a membrane at 25 °C. *D*, membrane-associated KRAS fractions, S_L, plotted as a function of the dissociation time. *E*, KRAS fraction, S_L, residual plot.
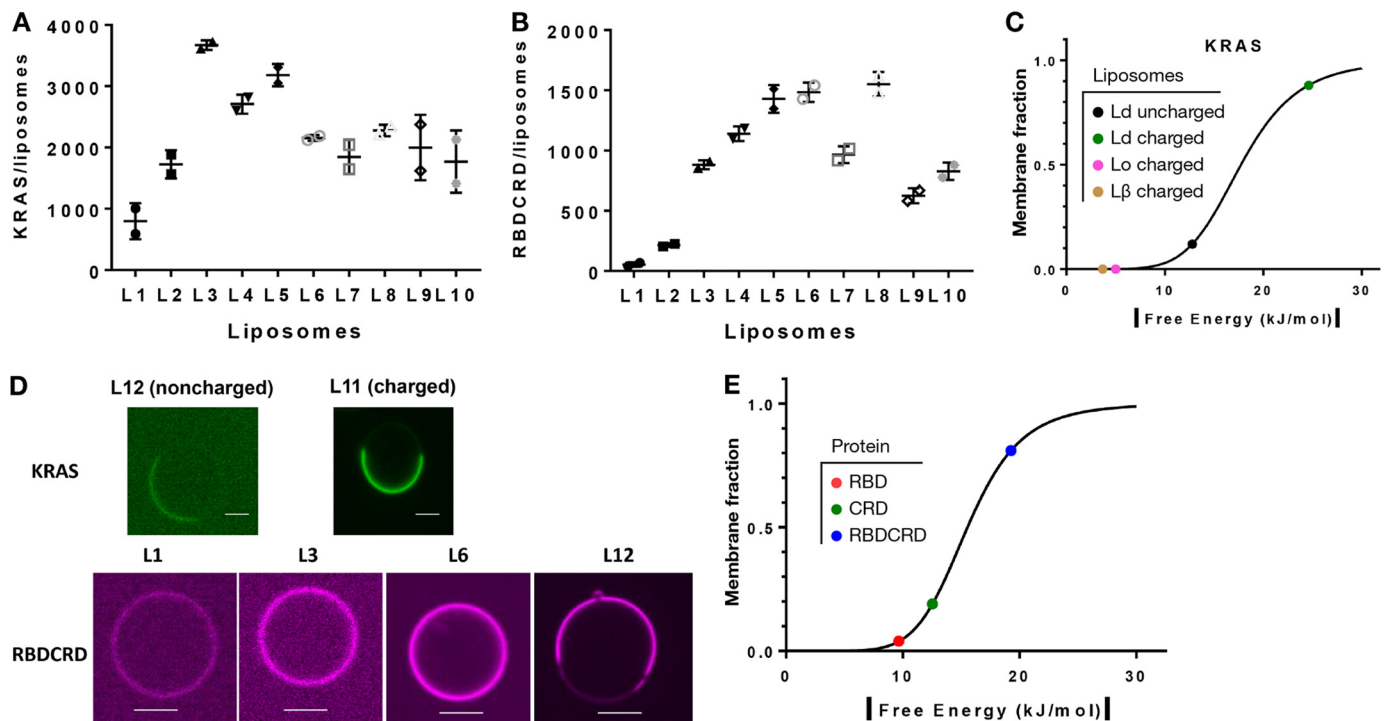

Figure 2. KRAS and RAF1 domains' membrane interaction. *A* and *B*, KRAS (*A*) and RBDCRD (*B*) protein per liposome (L1 to L10) stoichiometry values determined according to Equation 8 at 10 and 50 μM, respectively. *Error bars* are determined based on duplicate data. *C*, fraction of membrane-associated KRAS determined for four lipid compositions: L1 (Ld uncharged), L3 (Ld charged), L13 (Pβ' charged), and L14 (Lo charged). The free energies displayed for L13 and L14 are arbitrary values because KRAS did not partition in these two lipid compositions. *D, top panel*, confocal microscopy images of eGFP KRAS colocalizing in Ld phase of L12 noncharged (*left*) and L11 charged GUVs (*right*). *Scale bar* is 2.5 μm in length. *D, bottom panel*, confocal microscopy images of HaloTag Alexa Fluor 660 RBDCRD partitioning into GUV membranes (from left to right: L1, L3, L6, and Ld phase of L11 charged GUVs). *Scale bar* is 2.5 μm in length. *E*, RBD, CRD, and RBDCRD membrane-associated fraction on L6.
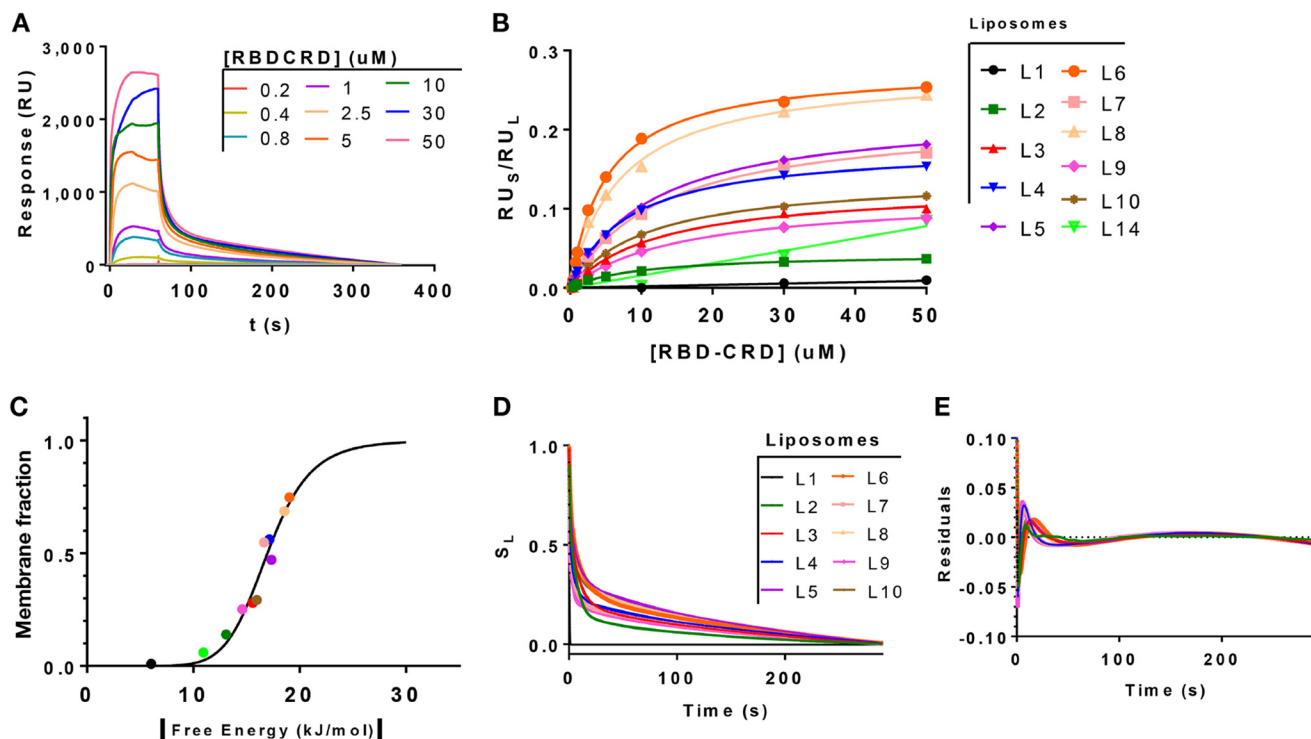
Figure 3. RBDCRD interaction with liposomes. *A*, SPR sensorgrams for RBDCRD partitioning into liposome L6. A baseline correction was applied to remove the retained fraction. *B*, binding isotherms for liposomes L1 to L10 and L14. RU_S values were collected from individual sensorgrams at 60 s of the association phase for each concentration. The RU_S values are displayed relative to RU_L values at each concentration for liposomes L1 to L10. *C*, RBDCRD membrane-associated fraction as a function of the absolute Gibbs free energy of transfer from the aqueous phase into a membrane at 25 °C. *D*, membrane-associated RBDCRD fractions, S_L, plotted as a function of the dissociation time. *E*, RBDCRD fraction, S_L, residual plot.

with 70 and 75% protein membrane associated for the replicates L6 and L8. It is also worth noting that RBDCRD showed less partitioning in liposomes containing DOPA than those containing DOPS (with the same net charge) a feature that was also observed for KRAS. Partitioning of the RAF domains in liquid ordered phases were investigated. SPR and imaging analysis using the L14 composition and L11 composition showed a clear preference of RBDCRD and CRD for disordered regions (Fig. 3, *B* and *C*). RBDCRD partitions at only about 7% in the liquid ordered region (Fig. 3*C*). RBDCRD Halo-tagged constructs showed detectable membrane localization via confocal imaging (Fig. 2*D*, *lower panel*) providing a qualitative visual representation of RBDCRD partitioning to the uncharged liposome L1 and some charged liposomes (L3, L6, L12).

An interaction driven by electrostatics should be modulated by varying the amount of $MgCl_2$ which is known for shielding charged lipids. We performed experiments with both CRD and RBDCRD at 0, 1, and 5 mM $MgCl_2$. A decrease in the $MgCl_2$ concentration clearly improved both CRD and RBDCRD partitioning (Fig. S4).

Not surprisingly, RBDCRD displays faster dissociation from the membrane than KRAS. Typically, for L3 negatively charged liposomes RBDCRD dissociates three times faster than KRAS with a weight-averaged half-life of 6 s compared with 18 s for KRAS. It also dissociates with a much faster dissociation rate from neutral DOPC membranes (approximately hundreds of milliseconds, close to the limit of detection) and combined fast and slow dissociating populations of RBDCRD were observed for all negatively charged liposomes (Fig. 3, *D* and *E* and Table

S1). Unlike KRAS, for RBDCRD the populations distribution seems to correlate with the negatively charged lipid ratio.

Ceramides have also been suggested to contribute to RAF1 partitioning through direct interaction with CRD (26). Non-charged liposomes containing various amounts of ceramides L15 and L16 were prepared and analyzed. The inclusion of ceramides did not increase membrane partitioning compared with DOPC alone, confirming the electrostatic nature of RBDCRD membrane interaction (Fig. S5).

HVR partitioning, dissociation, and secondary structure on liposomes

The hypervariable region of all RAS isoforms constitutes their primary anchor point to the membrane. In the case of KRAS, the presence of the polylysine stretch electrostatically drives the protein toward negatively charged lipids. The HVR and full-length KRAS show differences in their partitioning in negatively charged membranes (L3). KRAS partitions (83%) slightly better to the membrane than its membrane anchoring region (76%) (Fig. 4*A*). Interbilayer transfer combined with energy transfer-based approaches suggested that lipid-anchored macromolecules may dissociate from bilayers several-fold faster than the isolated anchor (27). Here we observe a similar trend whereby KRAS dissociates from L3 negatively charged membrane twice as fast as its isolated anchor (Fig. 4*D*). Both exhibit similar two-state dissociations with similar ~10 s fast half-lives. Weight-averaged half-lives differ by about 2-fold, 17 s and 35 s for HVR and KRAS, respectively.
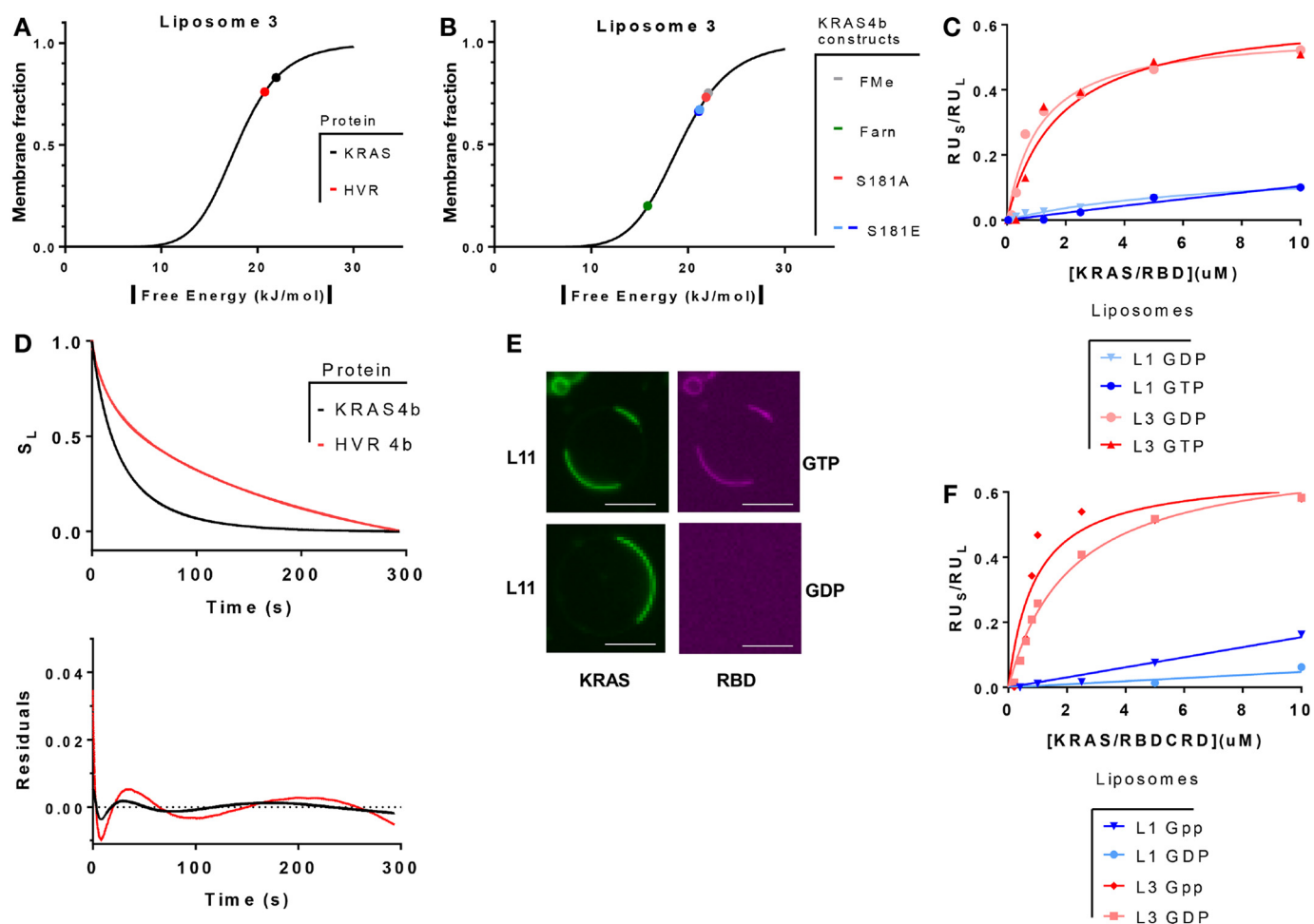
Figure 4. HVR and KRAS membrane interaction. *A*, fraction of membrane-associated KRAS and HVR protein as a function of the unitary Gibbs free energy of transfer from the aqueous phase into a membrane at 25 °C. *B*, fraction of membrane-associated KRAS for four different constructs on L3: KRAS, KRAS S181A, KRAS farnesylated only, and two replicates of KRAS S181E. *C* and *F*, binding isotherms of KRAS/RAF domains mixture partitioning into liposomes L1 and L3 using KRAS loaded with GDP or GppNHp (GTP analogue). RU_S values were collected from individual sensorgrams at 60 s of the association phase for each concentration. The RU_S values are displayed relative to RU_L values at each concentration for liposomes L1 and L3 for KRAS/RBD (*C*) or KRAS/RBDCRD (*F*), respectively. *D*, membrane-associated KRAS and HVR fractions, S_L, plotted as a function of the dissociation time. The residual plots are represented. *E*, confocal microscopy images of eGFP-KRAS and HaloTag Alexa Fluor 660-RBD partitioning into phase-separated L11 liposomes. Images were acquired with KRAS loaded with GppNHp or GDP. *Scale bar* is 2.5 μm in length.

Membrane-associated HVR secondary structure can give insights into the extent that each amino acid interacts with the membrane. Recently, the structure of the full HVR was solved in complex with the chaperone protein PDE6δ (28). In one of the two crystal forms the HVR is folded as an α-helix, suggesting that KRAS HVR is intrinsically able to fold into an α-helix. CD spectra obtained from HVR-associated neutral L1 and negatively charged L3 membranes exhibited a single minimum at 197 nm, which is indicative of unfolded proteins (Fig. S3*d*). Despite this measurement being an average of membrane-associated (76%) and aqueous species in equilibrium, the predominant unfolded signal strongly suggests that the HVR alone would be mostly disordered regardless of the membrane charge. It is worth noting that other small positively charged peptides demonstrate the ability to fold upon binding to negatively charged membranes under similar conditions (29).

Influence of posttranslational modifications on KRAS membrane partitioning

KRAS is subject to two major modifications that result in membrane localization. During its processing, the addition of an *O*-methylation to the C terminus of the terminal cysteine occurs in addition to the *S*-isoprenylation of the CAA*X* motif. Carboxymethylation has been shown to provide a decrease in free energy by ~6 kJ/mol, which increases the fraction of membrane-associated protein by ~60% with significant biological implications (19, 30). Our SPR platform delivers very similar results with a 6.2 kJ/mol free energy difference and a 55% increase in membrane-associated fraction between KRAS farnesylated methylated and KRAS farnesylated.

The importance of Ser-181 phosphorylation in KRAS is unclear, with some work reporting a weaker affinity for the membrane that results in decreased MAPK pathway activity (31, 32). Other studies support increased signaling because of a reorganization of KRAS at the membrane with minimal changes in membrane affinity (33, 34). To understand the effect of the phosphorylated Ser-181 KRAS two mutants at this position were tested for membrane partitioning: the phosphomimetic mutant S181E as well as the alanine mutant S181A. Because the recombinantly expressed and purified mutants were only 83% carboxymethylated (the remaining 17% was just farnesylated), the WT KRAS was diluted with farnesylated

Quantitative analysis of KRAS membrane interaction

KRAS only to achieve 83% total methylation in the sample. Two independent S181E samples were run and were 66% membrane-associated with a 1% difference between both samples. KRAS WT and the S181A neutral mutant were 75 and 73% membrane-associated, respectively (Fig. 4*B*). This ~10% difference on KRAS membrane localization seen at a biophysical level could have a significant impact on MAPK signaling pathway if similar in cells. Previous studies had demonstrated that Ser-181 phosphorylation does not dislodge KRAS immediately from the PM in cells (34). Our results quantify the reduced free energy of KRAS membrane partitioning because of the phosphorylation at Ser-181.

Previously, a combination of simulation and mutational analysis performed on HRAS led to a model where GTP- and GDP-bound KRAS would interact with the membrane differently, which could influence their relative membrane affinity (35). Here we tested for differential nucleotide-dependent affinity of KRAS and find no difference in membrane partitioning (Fig. S3*c*).

Effector modulation of KRAS membrane partitioning and dissociation

KRAS activates the MAPK pathway through GTP-dependent binding to RAF1. Understanding how this interaction might influence KRAS membrane partitioning properties requires complex experimental conditions. To probe this interaction, we injected equimolar mixtures of RBD or RBDCRD with KRAS containing either GDP or GppNHp. RBDCRD caused a slight increase in the membrane partition of KRAS-GppNHp compared with KRAS-GDP, however RBD had no impact in KRAS membrane partitioning (Fig. 4, *C* and *F*). This membrane partitioning increase of RBDCRD/KRAS complex can be attributed to the added membrane affinity contribution of RBDCRD. The nucleotide-dependent effect is noticeable both in negatively charged L3 membranes whereby KRAS/RBDCRD complex membrane-associated fraction increases from 82 to 88% and neutral membranes where this fraction increased from 8 to 22% (Fig. 4*F*). Confirmation of the nucleotide-dependent binding of RBD to KRAS was obtained by using a fluorescent-tagged HaloTag Alexa Fluor 660 RBD on phase-separated GUVs (Fig. 4*E*). A clear membrane relocation of RBD is noticed only when KRAS is loaded with GppNHp. It is worth noting here that at the concentrations used in this experiment no RBD membrane partitioning is detectable.

We also investigated other established and putative KRAS protein-binding partners for their ability to impact KRAS membrane-partitioning properties. Calmodulin is reported to specifically bind to KRAS and facilitate its dissociation from membranes independent of the nucleotide state (36–41). The structure of KRAS complexed with PDE6δ, the well-characterized farnesyl-binding protein, was recently solved (28). Galectin3 is proposed to be involved in KRAS distribution at the membrane (42–44), although no mechanism of action has yet been elucidated. Membrane partitioning of the three individual binding partners was tested first. No membrane partitioning into negatively charged L3 membrane was observed with calmodulin or PDE6δ. However, galectin3 showed a low-level membrane partitioning (data not shown). Mixtures of KRAS

and calmodulin at different calmodulin/KRAS molar ratios 0.12, 0.25, 0.37, 0.5, 0.65, 0.8, and 1 were injected on negatively charged L3 membranes. Direct comparison of relative binding isotherms at various molar ratios clearly shows that calmodulin decreases the amount of KRAS protein at the membrane at equilibrium (Fig. 5*A*). Similar experiments were performed with PDE6δ and galectin3 using chaperone/KRAS molar ratios of 0, 0.5, and 1 (Fig. 5*C*). PDE6δ was also able to decrease the amount of KRAS at the membrane at equilibrium; however, the inclusion of galectin3 resulted in a slight increase in overall partitioning. Fig. 5*E* displays the normalized stoichiometries (*i.e.* amount of KRAS molecules per liposome) which allows us to quantitatively compare the effect of each chaperone. As mentioned previously, for both calmodulin and PDE6δ, the stoichiometry decreases with increasing amounts of chaperones reaching normalized values of 0.36 and 0.66, respectively, at equimolar ratios. This difference between the two chaperones implies that calmodulin is more efficient at preventing KRAS membrane adsorption. The slight increase in stoichiometry in the presence of galectin3 is likely because of the small membrane partitioning of galectin3 itself. Phosphorylated KRAS at position 181 was proposed to inhibit calmodulin KRAS binding and consequently abolish calmodulin's effect on KRAS membrane partitioning (40, 41). The phosphomimetic mutant KRAS S181E was used in place of KRAS WT in a similar experimental format. Comparison of the normalized stoichiometry values showed that a phosphomimetic at Ser-181 on KRAS has no effect on calmodulin–KRAS membrane interplay (Fig. 5*E*).

Interestingly, this experimental set up showed that calmodulin also had an impact on KRAS dissociation rate. Although the weight-averaged half-life appeared to increase slightly, the population ratios are drastically affected by the gradual addition of calmodulin. The fast dissociating population decreasing from 45 to 0% (Table S2). PDE6δ showed a similar effect of decreasing KRAS dissociation at high PDE6δ concentrations with minimal changes on the populations (Fig. 5*C* and Table S2). Galectin3 influence on KRAS dissociation is plotted on Fig. 5*F*. However, no attempt was made to quantify this effect because of its convolution with galectin3 self-dissociation from the membrane.

Because the galectin3 results failed to show a significant impact on KRAS membrane interaction, we decided to analyze its direct interaction with KRAS at a biophysical level because most of the literature on galectin3 KRAS interaction relies on in-cell observation (45). Using a traditional protein-protein interaction approach by SPR, direct binding between galectin3, KRAS, and RAF1 RBD was investigated. No direct interaction was detected between galectin3 and KRAS or RBD up to 10 μM (Fig. S2, *a* and *b*). Injection of active KRAS/RBD complex onto galectin3 also did not show binding up to 10 μM (Fig. S2*c*). In addition, galectin3 had no effect on the binding of RBD to KRAS at concentrations up to 100 μM to RBD without affecting its K_D for active KRAS (Fig. S2*d*).

Discussion

We have developed an experimental format that enables the analysis of a panel of liposomes and uses SPR technology to extract quantitative parameters of the interaction between
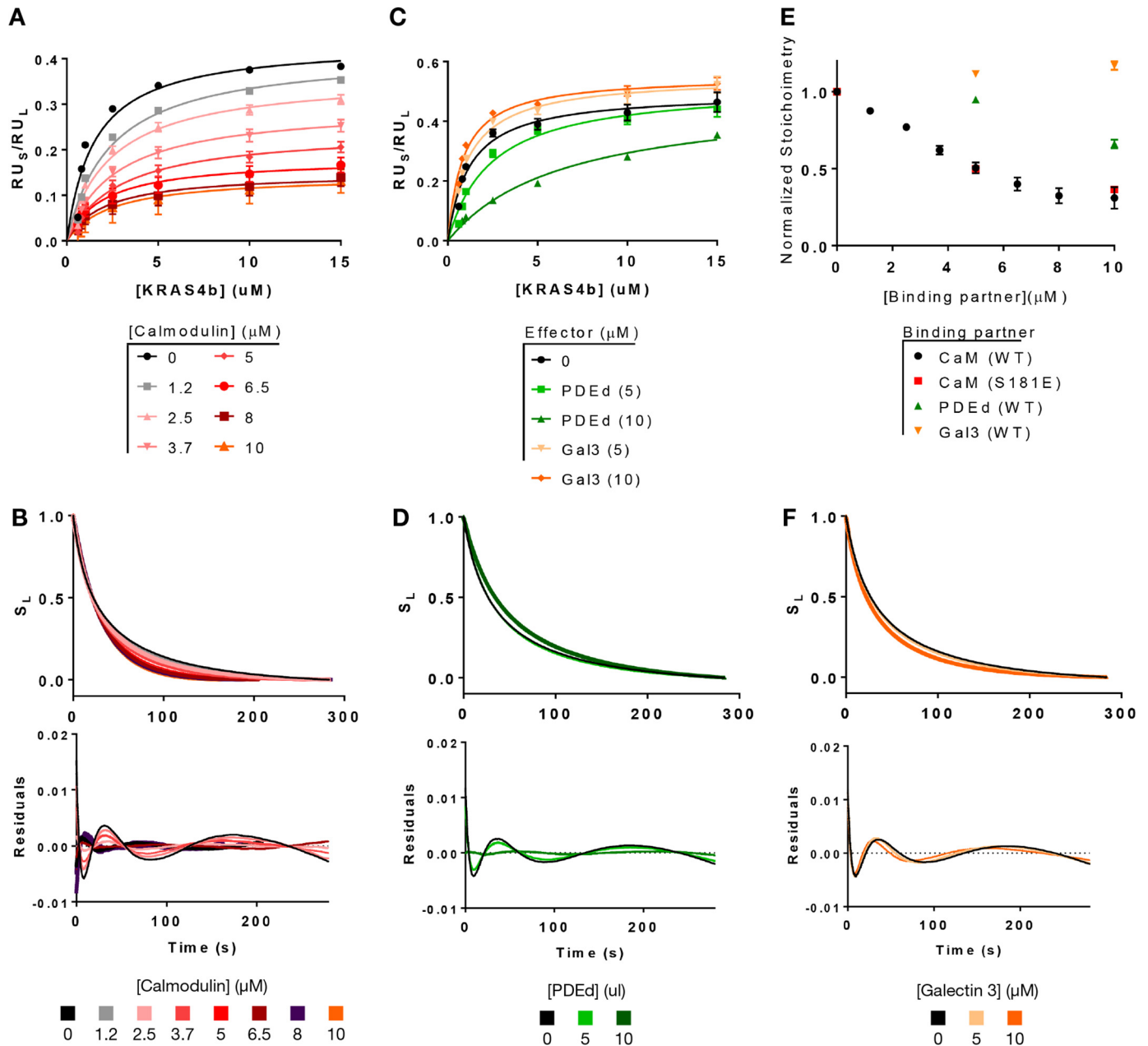
Figure 5. KRAS/chaperones membrane interaction. Binding isotherms of KRAS partitioning into liposome L3 in presence of various concentration of calmodulin, PDE6δ, or galectin3. The RU$_S$ values are displayed relative to RU$_L$ values at each concentration for KRAS/calmodulin (*A*) and KRAS/PDE6δ or KRAS/galectin3 (*C*), respectively. Membrane-associated KRAS/calmodulin (*B*), KRAS/PDE6δ (*D*), and KRAS/galectin3 (*F*) fractions, S$_L$, plotted as a function of the dissociation time. The respective residual plots are represented. *E*, normalized KRAS WT and KRAS S181E stoichiometry per L3 liposome as a function of various effectors concentration.

KRAS and a series of model membranes. One such parameter is the residence time. We show that KRAS spontaneously associates to and dissociates from the membrane with fast kinetics (seconds). For both KRAS and RBDCRD the presence of negatively charged lipids creates an additional dissociation rate that suggests the association and dissociation mechanisms involves at least two separate events: Initial membrane bilayer attachment through nonspecific electrostatic interaction responsible for the fast on-rate and slow off-rate followed by specific insertion of hydrophobic and aromatic residues into the interfacial and hydrocarbon core regions of the lipid bilayer. For KRAS this phenomenon has been well-studied and involves both elec-

trostatic adsorption of the polylysine repeat subsequently stabilized by insertion of the farnesyl moiety. A similar mechanism for RAF1 RBDCRD suggests a relatively deep insertion of hydrophobic amino acids following an initial nonspecific electrostatic membrane adsorption. Partial insertion of CRD in the hydrophobic core of the lipid bilayer via two hydrophobic loops was recently suggested by Travers *et al.* (46). Analysis of RAF1 domains reveals that RBD, CRD, and RBDCRD all contain excess positive charges and high isoelectric points 9.5, 8.9, and 9.2, respectively. The direct correlation between the population ratios of RBDCRD and charge ratio of the membrane along with the high pI supports the two-step hypothetical mechanism for
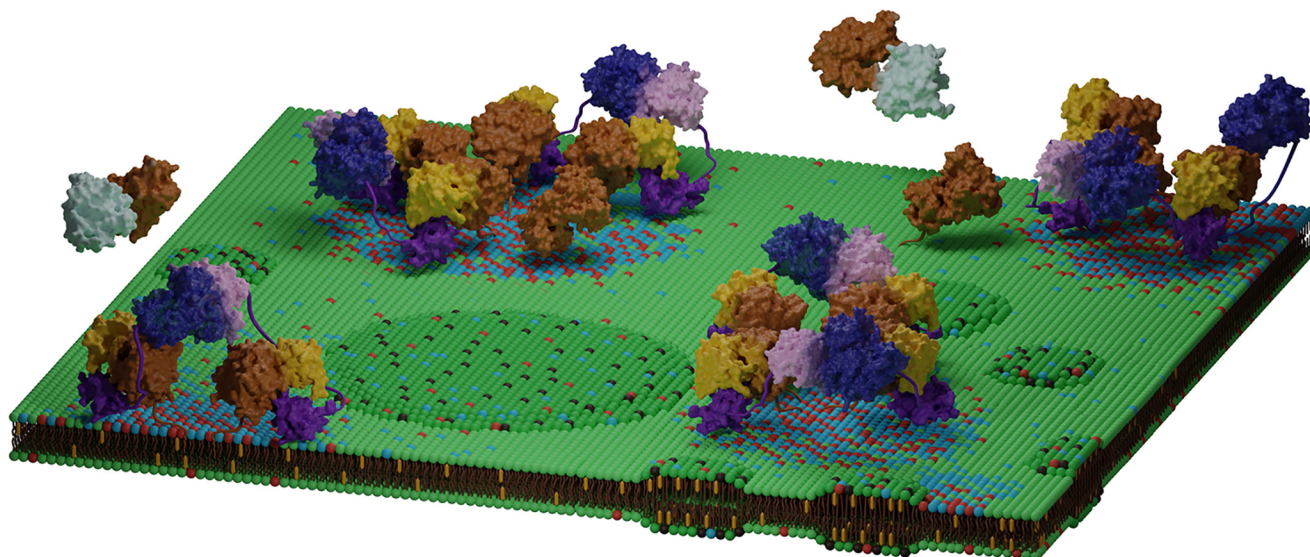
Figure 6. Model for KRAS/RAF interaction with the plasma membrane inner leaflet. KRAS (*brown*) (PDB ID: 5W22) is on and off the membrane. When not associated with the membrane, KRAS is passively sequestered by PDE6δ (*white*) (PDB ID: 5TAR) or calmodulin (not represented). At the membrane, KRAS mostly clusters in lipid microdomains containing high proportions of phosphatidyl serine (*blue headgroups*), phosphatidyl ethanolamine (*red headgroups*), or cholesterol (*yellow sticks*), and it clusters away from thicker liquid ordered domains that contain palmitoyl sphingomyelin lipids (*black headgroups*). The RAF CRD domain (*purple*) (PDB ID: 1FAR) mostly drives RAF membrane interaction, whereas the RAF RBD domain (*yellow*) (PDB ID: 4G0N) is bound to KRAS, and the RAF kinase domain dimerizes (*dark blue* and *pink*) (PDB ID: 3OMV) when two monomers (*dark blue*) (PDB ID: 5CSX) are near.

RBDCRD membrane interaction: (i) nonspecific electrostatic interaction and (ii) deeper insertion of hydrophobic residues.

KRAS exhibits a more complex adsorption/desorption mechanism revealed by the 2-fold increase in the slower dissociating population with respect to the liposome charge ratio. Such a difference implies an additional KRAS clustering triggered by the presence of negatively charged lipids or to a reorganization of the negatively charged lipids in microdomains that increases their contribution. The significant increase in membrane adsorbed KRAS molecules from neutral L1 liposomes (~500) to charged L3 liposomes (~3000) would allow such clustering to occur. It has also been observed both *in vitro* (29, 47) and *in vivo* (48, 49) that negatively charged lipids can enhance clustering of positively charged proteins and peptides at specific foci on membranes. It is worth noting that the HVR alone could trigger such a clustering event independent of residues in the G-domain. In such a scenario, the clustered fraction would undergo a slow dissociation and the isolated KRAS molecules would constitute the fast dissociating population. In this model the KRAS adsorption process would have three components: (i) nonspecific electrostatic interaction, (ii) deeper insertion of the farnesyl moiety, and (iii) reorganization of KRAS interacting lipids (*i.e.* PS, PE, cholesterol) into microdomains promoting KRAS molecules clustering (Fig. 6).

RAF1 CRD is essential for RAF1 membrane partitioning. For all lipid compositions tested, the CRD domain displayed better membrane partitioning than the RBD, suggesting that it is indeed driving the interaction with the membrane (Fig. 2*E*). To our surprise, the CRD domain exhibited very little membrane partitioning compared with the RBDCRD domain. Several hypotheses can support such a phenomenon. We showed that RBD and CRD individually partition with a low but nonnegligible free energy into negatively charged membranes (Fig. 2*E*). Combining both domains could multiply and thus enhance

their avidity. A structural hypothesis would suggest that proper folding of the CRD domain might not be possible as an isolated domain and requires association with its adjacent RBD sequence to adopt the proper lipid recognition motif.

The importance of a lipidated hypervariable region for membrane localization has been well-studied (5, 35, 50–52). On the negatively charged L3 liposomes, KRAS G-domain alone showed marginal membrane partition up to 100 μM (data not shown) confirming that membrane anchoring requires the hypervariable region. We also observed a 2-fold slower dissociation of HVR compared with KRAS which can be explained via two general mechanisms whereby a globular hydrophilic portion can influence the rate of conjugate desorption. First, the transfer of a molecule from a large complex to an aqueous solution generates a gain in translational and rotational entropy. Second, the adsorption of a flexible polymer to a bilayer will significantly lower its conformational entropy. The contribution of these two factors are predicted to scale with their molecular weights in the first case and their polymerization number in the second case (53, 54). This increased dissociation of KRAS with respect to its HVR portion is combined with an increase (between ~7 and 15%) in membrane partitioning for KRAS. This observation favors a contribution from G-domain residues in stabilizing the membrane adsorption as described previously (55). Using paramagnetic relaxation enhancement NMR to analyze tethered KRAS residues preferential orientation with respect to negatively charged nanodiscs, Ikura and co-workers (56) also suggested a contribution from specific residues in the G-domain that would favor, in a nucleotide-specific mechanism, two specific orientations of membrane-associated KRAS. Although this seems contradictory with the absence of membrane partitioning for a G-domain–only KRAS, it is possible that membrane localization is required for the G-domain residues to contribute.

It is worth noting that the uncertainty range in membrane partitioning between KRAS and HVR is a consequence of KRAS being recombinantly expressed and not 100% carboxymethylated contrary to the synthetic HVR peptide. Determination of the partition coefficient for the noncarboxymethylated KRAS confirmed that even small variations in carboxymethylation affect the overall membrane partitioning. Although only samples that were at least 85% methylated were used in this study, given the contribution of the methylation, an ~15% range has a noticeable impact. A G-domain contribution would also explain the only 2-fold difference in dissociation given the ~8-fold molecular weight difference between KRAS and HVR.

For all proteins the fractional membrane-associated values were plotted against free energy of membrane partitioning with nonlinear curves. This representation allows direct assessment of the contribution of lipids and protein modifications on the membrane protein fraction. The nonlinear fitting shows that a protein membrane-associated fraction is not linearly proportional to the free energy of membrane partitioning. Instead, depending on its membrane-binding characteristics and the membrane composition, each membrane-associated protein has a free energy of membrane partitioning required to give 50% membrane partitioning. At this free energy regime, minor contributions to the free energy impact the fractional value significantly.

To determine KRAS lipid preference we first analyzed the influence of the lipid polar headgroups. Our results confirm the importance of the electrostatics in KRAS membrane interaction. Interestingly, Fig. 1*C* shows how variation of the membrane charge state between 0 and 30% (~8 kJ/mol) affects KRAS membrane distribution. This agrees with cell-based studies in which KRAS is preferentially localized with the negatively charged plasma membrane compared with the less negatively charged endomembranes (57). Analysis of the KRAS stoichiometry and lipid to solute ratio σ results at saturation reveals that the two PS-containing lipid compositions which are cholesterol free can accommodate more KRAS molecules and thus showed lower σ (Table S3). Cholesterol is known to increase the packing of disordered bilayers, which explains how a more densely packed membrane accommodates fewer farnesyl moieties. The effect of the ordered/nonordered state of acyl chains on KRAS membrane interaction was also studied by increasing temperature. Decreased membrane partitioning of KRAS was observed at high temperature (Fig. S3). Although more disordered acyl chains favor better insertion of the farnesyl group, increasing the kinetic energy also disrupts biomolecular interactions (hydrogen bonds, electrostatic and hydrophobic interactions) and lowers KRAS membrane partitioning.

Comparison of the kinetics of KRAS desorption from the 10 different liposomes (L1–L10) recapitulating the general lipid headgroup composition of the inner leaflet suggests an increased amount of interaction decreasing the off-rate for some compositions. These additional interactions are more pronounced for the PE and cholesterol containing liposomes. Phosphatidylethanolamines are the most prevalent lipid headgroup in the inner leaflet. Their primary amine moiety's ability is to establish hydrogen bond interactions with other lipids but potentially also membrane-adsorbed proteins might explain

this slower rate of desorption. Cholesterol molecules increase packing in the membrane that might be involved in trapping the inserted farnesyl chains causing a delay in their release.

The suggestion that raft signaling platforms (58, 59) are important in the MAPK pathway is of interest because of raft's ability to segregate RAS isoforms into domains of various rigidity (2). Despite the inner leaflet being made of mostly polyunsaturated lipids, not subject to phase separation, visualization of inner leaflet microdomains in cells confirmed the existence of a mechanism for transferring the outer leaflet rigidity to the inner leaflet (60). Teres *et al.* (61) also observed weaker KRAS partitioning into cell membranes enriched in the raft forming lipid sphingomyelin compared with polyunsaturated PE lipids . Several studies demonstrated that the single farnesyl moiety of KRAS does not partition in raft signaling platforms or *in vitro* liquid ordered domain (6, 62). Analysis of L11 and L14 lipid compositions that generate liquid ordered domains using, both SPR and imaging confirmed the absence of KRAS partitioning in these raftlike domains.

In contrast to KRAS, RAF1 is a protein that is mainly localized in the cytoplasm. We showed that its membrane-interacting segment RBDCRD exhibits features of a membrane-associated protein. Consistent with the general properties of the full-length RAF1, RBDCRD showed faster desorption kinetics than KRAS. As seen for KRAS, RBDCRD dissociation only follows first-order kinetics for the neutral lipid composition which suggests that the fast component of the dissociation is because of dissociation from the neutral lipids and the slow component is caused by additional interaction with other lipids. Analysis of the half-lives based on the lipid composition seems to correlate with stronger interaction with PE containing liposomes. We believe that these interactions could be hydrogen bonding events with the protein. The distribution of the RBDCRD membrane-associated fractions over this range of lipid composition confirms that its interaction with the membrane is both electrostatic and stabilized by additional interaction with lipids such as PE and cholesterol. Contrary to KRAS, RBDCRD fractional membrane-associated values do not feature two separate populations of neutral and charged lipid compositions that display weak and good membrane partition, respectively. Instead, the fractional values corresponding to various lipid compositions are distributed along a nonlinear curve (Fig. 3*C*). This distribution suggests a differential contribution of the electrostatic interaction relative to free energy of membrane partitioning required to give 50% membrane partitioning. At this free energy regime, RBDCRD electrostatic contribution is less, giving contribution of other lipids such as PE and cholesterol a greater importance. However, by decreasing MgCl$_2$ and thereby changing the free energy regime we increased the contribution of the electrostatic interaction with respect to PE and cholesterol (Fig. S4*b*). Like KRAS in a liquid disordered phase, the addition of cholesterol also seemed to increase the fraction of membrane-associated RBDCRD suggesting a deep enough insertion for the cholesterol trapping mechanism to occur. Surprisingly, RBDCRD partitions in the liquid disordered region of phase separated vesicles. This observation, which was confirmed both by SPR and imaging in giant vesicles, dovetails with the relatively deep penetration of the protein for it to sense the

repulsive packing effect of the liquid ordered phase. Similarly, to KRAS, strong electrostatics are necessary but not sufficient to promote RBDCRD membrane partitioning. Efficient partitioning can only occur when the membrane is in a liquid disordered phase. The RAF1 kinase would therefore not be able to efficiently interact with putative raft domains. Interestingly, all active RAS isoforms are localized in the nonraft domains and artificially directing RAF1 to the opposite raftlike domain results in absence of MAPK signaling (63). The propensity of RAF1 and all active RAS isoforms to localize in similar lipid microdomains should increase interactions and synergize MAPK signaling. Because this RBDCRD domain is mostly conserved between RAF kinases isoforms, ARAF and BRAF could also behave similarly.

Contrary to a previous report (26), we did not observe RBDCRD binding to ceramide containing liposomes. This could be attributed to differences in experimental setups. Most reported work on CRD ceramide interaction were performed on platforms such as lipid stripes which do not reflect a physiological lamellar phase. Our observation suggests that CRD membrane partitioning is primarily electrostatically driven. Ceramides being neutral lipids would therefore not contribute significantly to RBDCRD partitioning.

RAS/RAF membrane localization is a critical step in MAPK pathway activation. Our data show a differential partitioning for RAS and RAF1 domains dictated by specific lipid headgroups. Beyond the electrostatic effect, PS containing lipids displayed better affinity than PA. Qualitative comparison of our results with an *in vitro* MEK phosphorylation activity assay developed by Jansen *et al.* (64) in which KRAS and MEK are added to a cell lysate containing BRAF in presence of various liposomes shows good correlation with their phospholipid dependences.

Because KRAS and RBDCRD both interact with negatively charged membranes, it is difficult to quantify the effect of RBDCRD on KRAS membrane interaction. Our results show that RBDCRD increases the membrane partitioning of KRAS/RBDCRD complexes in a GTP-dependent manner. This effect, which was detected for both charged and uncharged membranes, was not observed with the shorter RBD. Considering that RBDCRD has a stronger membrane affinity than RBD, this suggests that RBDCRD synergizes KRAS membrane partitioning when bound to it. Conversely, the RBD contribution to membrane partitioning would not be sufficient to modify KRAS/RBD complexes membrane partitioning properties. At the cellular level, it is likely that RAF1 kinase behaves like RBDCRD and potentially synergizes even more the KRAS membrane partitioning.

Previous *in vitro* studies showed that although PDE6δ can bind KRAS, it was not able to alter KRAS membrane interaction, suggesting that PDE6δ would dissociate from KRAS upon membrane partitioning (39, 65). Our data suggest that both calmodulin and PDE6δ can passively sequester the non–membrane-associated pool of KRAS (Fig. 5, *A, C,* and *E*). Analysis of KRAS remaining membrane fraction emphasizes that calmodulin passive sequestration is more efficient. Interestingly, dissociation analysis suggests that calmodulin tends to deplete the fast membrane dissociating KRAS pool whereas PDE6δ did not

show such selectivity (Fig. 5, *B* and *D*). PDE6δ effect on KRAS would therefore be only a passive sequestration in the cytoplasm of spontaneously dissociated KRAS from membranes whereas calmodulin effect would be more targeted toward the fast dissociating KRAS population.

Galectin3 is frequently mentioned as a KRAS chaperone that reorganizes KRAS membrane distribution (42, 45). Our results did not confirm any direct interplay between galectin3, RBD, and KRAS irrespective of nucleotide state (Fig. S2). It is worth noting that aside from *in vitro* FRET (45), no direct interaction has been detected between galectin3 and KRAS suggesting that the potential interplay between galectin3 and activated KRAS at the membrane might involve additional proteins as suggested by Cheresh and co-workers (66).

KRAS membrane interaction has been studied extensively in formats ranging from whole organisms to synthetic models. Comparison of these various studies is often difficult considering their experimental conditions and the various techniques used. Here we performed a comprehensive *in vitro* biophysical study to identify factors that influence KRAS/RAF1 membrane interaction by focusing on lipids constituting the PM inner leaflet and a selection of known or putative binding partners modulating KRAS recruitment to the PM. Our results show that KRAS and RAF1 domains interact with the membrane primarily through electrostatic interactions with negatively charged lipids reinforced by additional interactions involving phosphatidyl ethanolamine and cholesterol. RAF1 RBDCRD interacts with the membrane significantly stronger than the isolated RBD, CRD domains and synergizes KRAS membrane partitioning. Calmodulin and PDE6δ, but not galectin3, passively sequester KRAS and prevent it from partitioning into the PM. RAF1 RBDCRD interacts with membranes preferentially at nonraft lipid domains. The carboxyterminal *O*-methylation is crucial for KRAS membrane localization. These results better define how KRAS–membrane interaction can be tuned by multiple factors. These key factors that modulate KRAS–membrane interaction constitute targets that could lead to new drug discovery approaches aiming at disrupting this crucial interaction.

Experimental procedures

All lipids were purchased from Avanti Polar Lipids (Alabaster, AL): DOPC, DOPS, DOPE, DOPA, egg sphingomyelin (PSM), PIP2, cholesterol, POPC, POPS, egg ceramide, DPPS, and DPPC. KRAS4b 167–188 C-terminal farnesylated methylated peptide (hereafter referred to as HVR) was purchased from Anaspec. The DOPE labeled with Atto 647N (Atto 647 DOPE) was purchased from Sigma-Aldrich.

Constructs for protein expression were produced using Gateway recombination-based cloning as described previously by Esposito *et al.* (67) using either PCR-amplified products or synthetic DNA as starting materials. Destination vectors used were *Escherichia coli* T7–based expression vectors based on pET42 and incorporating various purification and solubility tags as noted in the supporting information. All clones were fully sequence verified throughout the insert regions.

Liposomes were prepared from lipid stock solutions in chloroform and mixed at the desired molar composition (c.f. Table 1). Most of the chloroform was evaporated in a gaseous nitro-

gen stream and afterward dried overnight under vacuum to remove the remaining solvent and then stored at 20 °C. Before the experiments, the lipids were resuspended in ~1 ml 20 mM HEPES buffer (pH 7.4), 5 mM MgCl$_2$, 150 mM NaCl, 1 mM TCEP and vortexed to yield a theoretical total lipid concentration of 6 mM. After hydration, the lipid solution was sonicated for 5 min at 40 °C (65 °C for the DPPC-containing mixtures) followed by five freeze-thaw-vortex cycles and another brief sonication. Large unilamellar vesicles (LUVs) were formed by extrusion through a polycarbonate filter with a 100-nm pore diameter. The extruded solution was then diluted to a concentration of 1 mM.

SPR experiments were carried out in a Biacore S200 instrument from GE Healthcare. Temperature was set at 25 °C or 37 °C for all experiments. A 20 mM HEPES, 150 mM NaCl, pH 7.4, 5 μM GDP with MgCl$_2$ ranging from 0 to 5 mM solution was used as running buffer for experiments using KRAS in the inactive state. Alternatively, GDP was replaced with 5 μM GppNHp for experiments using KRAS in the active state. The flow system was primed three times before initiating an experiment. The L1 sensor chip was used in all experiments. The sensor chip surface was rinsed with three injections of 20 mM CHAPS before LUV deposition. 1 mM lipid LUV samples were injected over the L1 sensor chip for 900 s, at a 2 μl/min flow rate. Typical RU values for DOPC, DOPC:DOPS (70:30), and DOPC:DOPS: DOPE:Chol (15:30:30:25) LUV depositions were ~7000, ~7000, and ~8,000, respectively. Loose vesicles were removed with a 36-s injection of 10 mM NaOH at 50 μl/min. Proteins at defined concentrations (between 0.2 and 50 μM) were injected over pre-formed lipid vesicle–coated surfaces at 30 μl/min, for a total of 60 s (association phase). Solutes were allowed to dissociate for 300 s. L1 sensor chip surface regeneration was performed with sequential injections of 20 mM CHAPS (5 μl/min for 60 s). Baseline response values were compared before and after each experiment to evaluate the effectiveness of the surface regeneration. Raw SPR sensorgram data were collected for both lipid deposition and solute binding. LUV deposition response values were collected from sensorgrams upon reaching a stable response. For each studied molecule, association steady-state response values were collected from individual sensorgrams at $t = 60$ s. Dissociation response data were collected between 60 and 360 s of each sensorgram.

Electroformation of giant unilamellar vesicles (GUVs) was performed according to published protocols (68, 69). To ensure mixing of all lipid components we performed electroformation at ~55 °C. Vesicles were electroformed in solution containing 350 mM sucrose (~350 mOsm). Lipids were mixed according to Table 1. After electroformation 1 μl of GUV solution was gently transferred to a homemade polydimethylsiloxane (PDMS, Sylgard) chamber containing 100 μl of protein solution (100 nM protein in 25 mM HEPES buffer with 150 mM KCl and 1 mM TCEP, 5 mM MgCl$_2$, osmotically balanced to 320 mOsm). The mixture was incubated at room temperature for 10 min and imaged immediately thereafter.

Halo-tagged proteins were incubated for 40 min with HaloTag Alexa Fluor 660 Ligand (Promega) at a 1:1.2 protein-to-dye ratio. The mixture was subsequently buffer exchanged into 20 mM HEPES, pH 7.3, 150 mM NaCl, 1 mM TCEP using a

prepacked PD-10 column as per the manufacturer's instructions. Halo-tagged proteins were then concentrated using an Amicon centrifugal filter device 10,000 MWCO at 4 °C.

GUVs were imaged on a spinning disc confocal microscope (Nikon) at 60× magnification (Zeiss, 63× Plan Apochromat 1.4 NA, oil), and analyzed using ImageJ (National Institutes of Health).

References

1. Cox, A. D., Fesik, S. W., Kimmelman, A. C., Luo, J., and Der, C. J. (2014) Drugging the undruggable RAS: Mission possible? *Nat. Rev. Drug Discov.* **13,** 828–851 CrossRef Medline
2. Prior, I. A., Harding, A., Yan, J., Sluimer, J., Parton, R. G., and Hancock, J. F. (2001) GTP-dependent segregation of H-ras from lipid rafts is required for biological activity. *Nat. Cell Biol.* **3,** 368–375 CrossRef Medline
3. Roy, S., Luetterforst, R., Harding, A., Apolloni, A., Etheridge, M., Stang, E., Rolls, B., Hancock, J. F., and Parton, R. G. (1999) Dominant-negative caveolin inhibits H-Ras function by disrupting cholesterol-rich plasma membrane domains. *Nat. Cell Biol.* **1,** 98–105 CrossRef Medline
4. Cho, W., and Stahelin, R. V. (2005) Membrane-protein interactions in cell signaling and membrane trafficking. *Annu. Rev. Biophys. Biomol. Struct.* **34,** 119–151 CrossRef Medline
5. Hancock, J. F., Paterson, H., and Marshall, C. J. (1990) A polybasic domain or palmitoylation is required in addition to the CAAX motif to localize p21ras to the plasma membrane. *Cell* **63,** 133–139 CrossRef Medline
6. Weise, K., Kapoor, S., Denter, C., Nikolaus, J., Opitz, N., Koch, S., Triola, G., Herrmann, A., Waldmann, H., and Winter, R. (2011) Membrane-mediated induction and sorting of K-Ras microdomain signaling platforms. *J. Am. Chem. Soc.* **133,** 880–887 CrossRef Medline
7. Mizutani, S., Inouye, K., Koide, H., and Kaziro, Y. (2001) Involvement of B-Raf in Ras-induced Raf-1 activation. *FEBS Lett.* **507,** 295–298 CrossRef Medline
8. Moravcevic, K., Mendrola, J. M., Schmitz, K. R., Wang, Y. H., Slochower, D., Janmey, P. A., and Lemmon, M. A. (2010) Kinase associated-1 domains drive MARK/PAR1 kinases to membrane targets by binding acidic phospholipids. *Cell* **143,** 966–977 CrossRef Medline
9. Nan, X., Tamgüney, T. M., Collisson, E. A., Lin, L. J., Pitt, C., Galeas, J., Lewis, S., Gray, J. W., McCormick, F., and Chu, S. (2015) Ras-GTP dimers activate the mitogen-activated protein kinase (MAPK) pathway. *Proc. Natl. Acad. Sci. U.S.A.* **112,** 7996–8001 CrossRef Medline
10. Besenicar, M., Macek, P., Lakey, J. H., and Anderluh, G. (2006) Surface plasmon resonance in protein-membrane interactions. *Chem. Phys. Lipids* **141,** 169–178 CrossRef Medline
11. Figueira, T. N., Freire, J. M., Cunha-Santos, C., Heras, M., Gonçalves, J., Moscona, A., Porotto, M., Salomé Veiga, A., and Castanho, M. A. (2017)

Quantitative analysis of molecular partition towards lipid membranes using surface plasmon resonance. *Sci. Rep.* **7,** 45647 CrossRef Medline

12. Zhou, Y., Prakash, P., Liang, H., Cho, K. J., Gorfe, A. A., and Hancock, J. F. (2017) Lipid-sorting specificity encoded in K-Ras membrane anchor regulates signal output. *Cell* **168,** 239–251.e216 CrossRef Medline

13. Wiener, M. C., and White, S. H. (1992) Structure of a fluid dioleoylphosphatidylcholine bilayer determined by joint refinement of x-ray and neutron diffraction data. III. Complete structure. *Biophys. J.* **61,** 434–447 CrossRef Medline

14. Sampaio, J. L., Gerl, M. J., Klose, C., Ejsing, C. S., Beug, H., Simons, K., and Shevchenko, A. (2011) Membrane lipidome of an epithelial cell line. *Proc. Natl. Acad. Sci. U.S.A.* **108,** 1903–1907 CrossRef Medline

15. van Meer, G., Voelker, D. R., and Feigenson, G. W. (2008) Membrane lipids: Where they are and how they behave. *Nat. Rev. Mol. Cell Biol.* **9,** 112–124 CrossRef Medline

16. Gillette, W. K., Esposito, D., Abreu Blanco, M., Alexander, P., Bindu, L., Bittner, C., Chertov, O., Frank, P. H., Grose, C., Jones, J. E., Meng, Z., Perkins, S., Van, Q., Ghirlando, R., Fivash, M., Nissley, D. V., McCormick, F., Holderfield, M., and Stephen, A. G. (2015) Farnesylated and methylated KRAS4b: High yield production of protein suitable for biophysical studies of prenylated protein-lipid interactions. *Sci. Rep.* **5,** 15916 CrossRef Medline

17. Ben-Tal, N., Honig, B., Peitzsch, R. M., Denisov, G., and McLaughlin, S. (1996) Binding of small basic peptides to membranes containing acidic lipids: Theoretical models and experimental results. *Biophys. J.* **71,** 561–575 CrossRef Medline

18. Ghomashchi, F., Zhang, X., Liu, L., and Gelb, M. H. (1995) Binding of prenylated and polybasic peptides to membranes: Affinities and intervesicle exchange. *Biochemistry* **34,** 11910–11918 CrossRef Medline

19. Silvius, J. R., and l'Heureux, F. (1994) Fluorimetric evaluation of the affinities of isoprenylated peptides for lipid bilayers. *Biochemistry* **33,** 3014–3022 CrossRef Medline

20. Erwin, N., Patra, S., Dwivedi, M., Weise, K., and Winter, R. (2016) Influence of isoform-specific Ras lipidation motifs on protein partitioning and dynamics in model membrane systems of various complexity. *Biol. Chem.* **398,** 547–563 CrossRef Medline

21. Erwin, N., Sperlich, B., Garivet, G., Waldmann, H., Weise, K., and Winter, R. (2016) Lipoprotein insertion into membranes of various complexity: Lipid sorting, interfacial adsorption and protein clustering. *Phys. Chem. Chem. Phys.* **18,** 8954–8962 CrossRef Medline

22. Werkmüller, A., Triola, G., Waldmann, H., and Winter, R. (2013) Rotational and translational dynamics of ras proteins upon binding to model membrane systems. *Chemphyschem* **14,** 3698–3705 CrossRef Medline

23. Ghosh, S., Strum, J. C., Sciorra, V. A., Daniel, L., and Bell, R. M. (1996) Raf-1 kinase possesses distinct binding domains for phosphatidylserine and phosphatidic acid. Phosphatidic acid regulates the translocation of Raf-1 in 12-*O*-tetradecanoylphorbol-13-acetate-stimulated Madin-Darby canine kidney cells. *J. Biol. Chem.* **271,** 8472–8480 CrossRef Medline

24. Ghosh, S., Xie, W. Q., Quest, A. F., Mabrouk, G. M., Strum, J. C., and Bell, R. M. (1994) The cysteine-rich region of raf-1 kinase contains zinc, translocates to liposomes, and is adjacent to a segment that binds GTP-ras. *J. Biol. Chem.* **269,** 10000–10007 Medline

25. Kraft, C. A., Garrido, J. L., Fluharty, E., Leiva-Vega, L., and Romero, G. (2008) Role of phosphatidic acid in the coupling of the ERK cascade. *J. Biol. Chem.* **283,** 36636–36645 CrossRef Medline

26. Yin, X., Zafrullah, M., Lee, H., Haimovitz-Friedman, A., Fuks, Z., and Kolesnick, R. (2009) A ceramide-binding C1 domain mediates kinase suppressor of ras membrane translocation. *Cell Physiol. Biochem.* **24,** 219–230 CrossRef Medline

27. Silvius, J. R., and Zuckermann, M. J. (1993) Interbilayer transfer of phospholipid-anchored macromolecules via monomer diffusion. *Biochemistry* **32,** 3153–3161 CrossRef Medline

28. Dharmaiah, S., Bindu, L., Tran, T. H., Gillette, W. K., Frank, P. H., Ghirlando, R., Nissley, D. V., Esposito, D., McCormick, F., Stephen, A. G., and Simanshu, D. K. (2016) Structural basis of recognition of farnesylated and methylated KRAS4b by PDEδ. *Proc. Natl. Acad. Sci. U.S.A.* **113,** E6766–E6775 CrossRef Medline

29. Jean-François, F., Castano, S., Desbat, B., Odaert, B., Roux, M., Metz-Boutigue, M. H., and Dufourc, E. J. (2008) Aggregation of cateslytin β-sheets on negatively charged lipids promotes rigid membrane domains. A new mode of action for antimicrobial peptides? *Biochemistry* **47,** 6394–6402 CrossRef Medline

30. Hancock, J. F., Cadwallader, K., and Marshall, C. J. (1991) Methylation and proteolysis are essential for efficient membrane binding of prenylated p21K-ras(B). *EMBO J.* **10,** 641–646 CrossRef Medline

31. Bivona, T. G., Quatela, S. E., Bodemann, B. O., Ahearn, I. M., Soskis, M. J., Mor, A., Miura, J., Wiener, H. H., Wright, L., Saba, S. G., Yim, D., Fein, A., Pérez de Castro, I., Li, C., Thompson, C. B., Cox, A. D., and Philips, M. R. (2006) PKC regulates a farnesyl-electrostatic switch on K-Ras that promotes its association with Bcl-XL on mitochondria and induces apoptosis. *Mol. Cell* **21,** 481–493 CrossRef Medline

32. Sung, P. J., Tsai, F. D., Vais, H., Court, H., Yang, J., Fehrenbacher, N., Foskett, J. K., and Philips, M. R. (2013) Phosphorylated K-Ras limits cell survival by blocking Bcl-xL sensitization of inositol trisphosphate receptors. *Proc. Natl. Acad. Sci. U.S.A.* **110,** 20593–20598 CrossRef Medline

33. Alvarez-Moya, B., López-Alcalá, C., Drosten, M., Bachs, O., and Agell, N. (2010) K-Ras4B phosphorylation at Ser181 is inhibited by calmodulin and modulates K-Ras activity and function. *Oncogene* **29,** 5911–5922 CrossRef Medline

34. Cho, K. J., Casteel, D. E., Prakash, P., Tan, L., van der Hoeven, D., Salim, A. A., Kim, C., Capon, R. J., Lacey, E., Cunha, S. R., Gorfe, A. A., and Hancock, J. F. (2016) AMPK and eNOS signaling regulates K-Ras plasma membrane interactions via cGMP-dependent protein kinase 2. *Mol. Cell. Biol.* **36,** 3086–3099 CrossRef Medline

35. Abankwa, D., Gorfe, A. A., Inder, K., and Hancock, J. F. (2010) Ras membrane orientation and nanodomain localization generate isoform diversity. *Proc. Natl. Acad. Sci. U.S.A.* **107,** 1130–1135 CrossRef Medline

36. Abraham, S. J., Nolet, R. P., Calvert, R. J., Anderson, L. M., and Gaponenko, V. (2009) The hypervariable region of K-Ras4B is responsible for its specific interactions with calmodulin. *Biochemistry* **48,** 7575–7583 CrossRef Medline

37. Fivaz, M., and Meyer, T. (2005) Reversible intracellular translocation of KRas but not HRas in hippocampal neurons regulated by Ca²⁺/calmodulin. *J. Cell Biol.* **170,** 429–441 CrossRef Medline

38. Sidhu, R. S., Clough, R. R., and Bhullar, R. P. (2003) Ca²⁺/calmodulin binds and dissociates K-RasB from membrane. *Biochem. Biophys. Res. Commun.* **304,** 655–660 CrossRef Medline

39. Sperlich, B., Kapoor, S., Waldmann, H., Winter, R., and Weise, K. (2016) Regulation of K-Ras4B membrane binding by calmodulin. *Biophys. J.* **111,** 113–122 CrossRef Medline

40. Villalonga, P., López-Alcalá, C., Bosch, M., Chiloeches, A., Rocamora, N., Gil, J., Marais, R., Marshall, C. J., Bachs, O., and Agell, N. (2001) Calmodulin binds to K-Ras, but not to H- or N-Ras, and modulates its downstream signaling. *Mol. Cell. Biol.* **21,** 7345–7354 CrossRef Medline

41. Wang, M. T., Holderfield, M., Galeas, J., Delrosario, R., To, M. D., Balmain, A., and McCormick, F. (2015) K-Ras promotes tumorigenicity through suppression of non-canonical Wnt signaling. *Cell* **163,** 1237–1251 CrossRef Medline

42. Elad-Sfadia, G., Haklai, R., Balan, E., and Kloog, Y. (2004) Galectin-3 augments K-Ras activation and triggers a Ras signal that attenuates ERK but not phosphoinositide 3-kinase activity. *J. Biol. Chem.* **279,** 34922–34930 CrossRef

43. Shalom-Feuerstein, R., Plowman, S. J., Rotblat, B., Ariotti, N., Tian, T., Hancock, J. F., and Kloog, Y. (2008) K-ras nanoclustering is subverted by overexpression of the scaffold protein galectin-3. *Cancer Res.* **68,** 6608–6616 CrossRef Medline

44. Tian, T., Plowman, S. J., Parton, R. G., Kloog, Y., and Hancock, J. F. (2010) Mathematical modeling of K-Ras nanocluster formation on the plasma membrane. *Biophys. J.* **99,** 534–543 CrossRef Medline

45. Blaževitš, O., Mideksa, Y. G., Šolman, M., Ligabue, A., Ariotti, N., Nakhaeizadeh, H., Fansa, E. K., Papageorgiou, A. C., Wittinghofer, A., Ahmadian, M. R., and Abankwa, D. (2016) Galectin-1 dimers can scaffold Raf-effectors to increase H-ras nanoclustering. *Sci. Rep.* **6,** 24165 CrossRef Medline

ASBMB

46. Travers, T., López, C. A., Van, Q. N., Neale, C., Tonelli, M., Stephen, A. G., and Gnanakaran, S. (2018) Molecular recognition of RAS/RAF complex at the membrane: Role of RAF cysteine-rich domain. *Sci. Rep.* **8,** 8461 CrossRef Medline

47. Jean-François, F., Desbat, B., and Dufourc, E. J. (2009) Selectivity of cateslytin for fungi: The role of acidic lipid-ergosterol membrane fluidity in antimicrobial action. *FASEB J.* **23,** 3692–3701 CrossRef Medline

48. Zhou, Y., and Hancock, J. F. (2015) Ras nanoclusters: Versatile lipid-based signaling platforms. *Biochim. Biophys. Acta* **1853,** 841–849 CrossRef Medline

49. Zhou, Y., Wong, C. O., Cho, K. J., van der Hoeven, D., Liang, H., Thakur, D. P., Luo, J., Babic, M., Zinsmaier, K. E., Zhu, M. X., Hu, H., Venkatachalam, K., and Hancock, J. F. (2015) Signal Transduction. Membrane potential modulates plasma membrane phospholipid dynamics and K-Ras signaling. *Science* **349,** 873–876 CrossRef Medline

50. Janosi, L., Li, Z., Hancock, J. F., and Gorfe, A. A. (2012) Organization, dynamics, and segregation of Ras nanoclusters in membrane domains. *Proc. Natl. Acad. Sci. U.S.A.* **109,** 8097–8102 CrossRef Medline

51. Prakash, P., Zhou, Y., Liang, H., Hancock, J. F., and Gorfe, A. A. (2016) Oncogenic K-Ras binds to an anionic membrane in two distinct orientations: A molecular dynamics analysis. *Biophys. J.* **110,** 1125–1138 CrossRef Medline

52. Zhou, Y., Liang, H., Rodkey, T., Ariotti, N., Parton, R. G., and Hancock, J. F. (2014) Signal integration by lipid-mediated spatial cross talk between Ras nanoclusters. *Mol. Cell. Biol.* **34,** 862–876 CrossRef Medline

53. Whittington, S. G. (1975) Self-avoiding walks terminally attached to an interface. *J. Chem. Phys.* **63,** 779 CrossRef

54. Finkelstein, A. V., and Janin, J. (1989) The price of lost freedom: Entropy of bimolecular complex formation. *Protein Eng.* **3,** 1–3 CrossRef Medline

55. Abankwa, D., Hanzal-Bayer, M., Ariotti, N., Plowman, S. J., Gorfe, A. A., Parton, R. G., McCammon, J. A., and Hancock, J. F. (2008) A novel switch region regulates H-ras membrane orientation and signal output. *EMBO J.* **27,** 727–735 CrossRef Medline

56. Mazhab-Jafari, M. T., Marshall, C. B., Smith, M. J., Gasmi-Seabrook, G. M., Stathopulos, P. B., Inagaki, F., Kay, L. E., Neel, B. G., and Ikura, M. (2015) Oncogenic and RASopathy-associated K-RAS mutations relieve membrane-dependent occlusion of the effector-binding site. *Proc. Natl. Acad. Sci. U.S.A.* **112,** 6625–6630 CrossRef Medline

57. Schmick, M., Vartak, N., Papke, B., Kovacevic, M., Truxius, D. C., Rossmannek, L., and Bastiaens, P. I. H. (2014) KRas localizes to the plasma membrane by spatial cycles of solubilization, trapping and vesicular transport. *Cell* **157,** 459–471 CrossRef Medline

58. Pike, L. J. (2003) Lipid rafts: bringing order to chaos. *J. Lipid Res.* **44,** 655–667 CrossRef Medline

59. Simons, K., and Toomre, D. (2000) Lipid rafts and signal transduction. *Nat. Rev. Mol. Cell Biol.* **1,** 31–39 CrossRef Medline

60. Prior, I. A., Muncke, C., Parton, R. G., and Hancock, J. F. (2003) Direct visualization of Ras proteins in spatially distinct cell surface microdomains. *J. Cell Biol.* **160,** 165–170 CrossRef Medline

61. Terés, S., Lladó, V., Higuera, M., Barceló-Coblijn, G., Martin, M. L., Noguera-Salvà, M. A., Marcilla-Etxenike, A., García-Verdugo, J. M., Soriano-Navarro, M., Saus, C., Gómez-Pinedo, U., Busquets, X., and Escribá, P. V. (2012) 2-Hydroxyoleate, a nontoxic membrane binding anticancer drug, induces glioma cell differentiation and autophagy. *Proc. Natl. Acad. Sci. U.S.A.* **109,** 8489–8494 CrossRef Medline

62. Wang, T. Y., Leventis, R., and Silvius, J. R. (2000) Fluorescence-based evaluation of the partitioning of lipids and lipidated peptides into liquid-ordered lipid microdomains: A model for molecular partitioning into "lipid rafts." *Biophys. J.* **79,** 919–933 CrossRef Medline

63. Inder, K., Harding, A., Plowman, S. J., Philips, M. R., Parton, R. G., and Hancock, J. F. (2008) Activation of the MAPK module from different spatial locations generates distinct system outputs. *Mol. Biol. Cell* **19,** 4776–4784 CrossRef Medline

64. Jansen, J. M., Wartchow, C., Jahnke, W., Fong, S., Tsang, T., Pfister, K., Zavorotinskaya, T., Bussiere, D., Cheng, J. M., Crawford, K., Dai, Y., Dove, J., Fang, E., Feng, Y., Florent, J. M., *et al.* (2017) Inhibition of prenylated KRAS in a lipid environment. *PLoS One* **12,** e0174706 CrossRef Medline

65. Weise, K., Kapoor, S., Werkmüller, A., Möbitz, S., Zimmermann, G., Triola, G., Waldmann, H., and Winter, R. (2012) Dissociation of the K-Ras4B/PDEδ complex upon contact with lipid membranes: Membrane delivery instead of extraction. *J. Am. Chem. Soc.* **134,** 11503–11510 CrossRef Medline

66. Seguin, L., Kato, S., Franovic, A., Camargo, M. F., Lesperance, J., Elliott, K. C., Yebra, M., Mielgo, A., Lowy, A. M., Husain, H., Cascone, T., Diao, L., Wang, J., Wistuba, I. I., Heymach, J. V., Lippman, S. M., Desgrosellier, J. S., Anand, S., Weis, S. M., and Cheresh, D. A. (2014) An integrin β_3-KRAS-RalB complex drives tumour stemness and resistance to EGFR inhibition. *Nat. Cell Biol.* **16,** 457–468 CrossRef Medline

67. Esposito, D., Garvey, L. A., and Chakiath, C. S. (2009) Gateway cloning for protein expression. *Methods Mol. Biol.* **498,** 31–54 CrossRef Medline

68. Angelova, M. I., and Dimitrov, D. S. (1986) Liposome electroformation. *Faraday Discuss. Chem. Soc.* **81,** 303–311 CrossRef

69. Schmid, E. M., Richmond, D. L., and Fletcher, D. A. (2015) Reconstitution of proteins on electroformed giant unilamellar vesicles. *Methods Cell Biol.* **128,** 319–338 CrossRef Medline